Jurnal Ilmu Fisika
Vol. 16, No. 2, September 2024, pp. 97–106
ISSN: 1979-4657 (Print); 2614-7386 (Online)
https://doi.org/10.25077/jif.16.2.97-106.2024

Jurnal Ilmu Fisika
Open Access

Characterization of Silicon from Rice Husk Doped with Cobalt: Analysis of Structure and Magnetoelectric Properties

Rizky Kurniawan[1,2], Andriayani Andriayani[3], Saharman Gea[3], Hadi Kurniawan[4]
[1] Department of Chemistry, Universitas Sumatera Utara, Medan, 20155, Indonesia
[2] Laboratory Faculty of Science and Technology, Universitas Islam Negeri Ar-Raniry, Banda Aceh, 23111, Indonesia
[3] Department of Chemistry, Universitas Sumatera Utara, Medan, 20155, Indonesia
[4] Department of Engineering Physics, Universitas Islam Negeri Ar-Raniry Banda Aceh, 23111, Indonesia

Article Info

Article History:

Received January 09, 2024
Revised March 18, 2024
Accepted April 07, 2024
Published online April 25, 2024

Keywords:

rice husk
silica
silicon
cobalt-doped silicon
magnetoelectric

Corresponding Author:

Andriayani Andriayani,
Email: andriayani@usu.ac.id

ABSTRACT

The development of Si-based materials has attracted increasing attention, particularly for application in semiconductors, batteries, sensors, and optical technology. Silicon has abundant availability, high energy storage capacity, and low work potential. However, it faces compatibility challenges due to its low electrical conductivity and extremely small magnetic susceptibility. This research aimed to investigate the influence of Co dopants on the structure, morphology, electrical conductivity, and magnetic susceptibility of silicon. Silicon was synthesized using the magnesiothermic reduction method, and silicon was modified with Co metal dopants at 0.1% and 0.5% concentrations through the impregnation method. XRD analysis results showed that Si, 0.1% Co/Si, and 0.5% Co/Si exhibit silicon diffraction patterns at 2θ = 28.42º; 47.28º; 56.11º; 69.13º; and 76.36º. The morphology of Si and Co/Si revealed a rough, uneven, and porous surface with particles appearing spherical. Electrical conductivity increases with Co concentration: Si = 1223 µS/cm, 0.1% Co/Si= 1376 µS/cm, and 0.5% Co/Si= 1529 µS/cm. Magnetic susceptibility measurements indicated that Si, 0.1% Co/Si, and 0.5% Co/Si are paramagnetic at a range of 1.18 x10^{-6} to 1.25 x10^{-5} SI. These characterization results confirmed that the modification with Co dopants can enhance the magnetoelectric properties of silicon.

1. INTRODUCTION

Silicon (Si) is one of the promising materials with potential applications in various industries, such as semiconductor technology, batteries, renewable energy, sensors, and optical technology (Margalit et al., 2021; Nulu et al., 2021). This material is abundant, has high energy storage capacity, enables the conversion of solar energy into electricity and is highly sensitive to various physical or chemical changes in the environment (Baig et al., 2021; Saif et al., 2023). Si is not found in its simple form in nature but is commonly encountered in the form of silicon dioxide (SiO_2), which can be sourced from sand, volcanic materials, clay, to sediments produced from mining processes (Andriayani et al., 2014; Thio et al., 2021). Additionally, other sources of Si are also found in the waste of organic materials such as rice husk ash, sugarcane bagasse, and bamboo (Daulay et al., 2022). Rice husk ash contains 80-97% silica, making it suitable for use as a raw material for Si production (Kaleli et al., 2020).

Currently, several methods have been reported for silicon production, such as chemical vapor deposition (CVD), metal-assisted chemical etching (MACE), and magnesiothermic reduction (MR) (Xu et al., 2017). These synthesis methods can yield Si with different properties and structures, including morphology, porosity, density, and crystallinity (Kiran et al., 2020). The MR approach is considered more advantageous as it seldom requires costly precursors, intricate equipment, and can utilize naturally occurring materials like rice husk ash and sand. Furthermore, the MR method after the silica reduction process, generates silicon material with a porous structure (Tan et al., 2021).

The crystalline structure of silicon adopts a diamond form with a density of 2.328 g/cm^3. Additionally, silicon possesses a bandgap energy of 1.12 eV, a melting point of 1415°C, a refractive index of 3.4, thermal conductivity of 1.5 W/cm°C, and electrical conductivity of 4.01×10^{-6}/Ωcm (Ng, 2002; Kumar & Johari, 2020; Tan, 2022). Nevertheless, silicon faces challenges in practical applications because it requires materials with properties unattainable with silicon, such as those enabling exceptionally high electrical conductivity (Nulu et al., 2022) or possessing unique optical characteristics (Dohnalová & Kůsová, 2021). Within the pure silicon structure, each silicon atom forms covalent bonds with other silicon atoms. The electrons involved in these bonds establish singular covalent bonds and are shared across silicon atoms (Tan, 2022). Consequently, silicon exhibits a low count of charge carriers (free electrons and holes), resulting in a restricted availability of carriers for electrical current conduction, contributing to the relatively modest electrical conductivity of silicon (Kumar & Johari, 2020).

Furthermore, silicon is recognized for its non-magnetic characteristics. At the atomic scale, silicon possesses a crystal structure devoid of directed magnetic domains or a macroscopic magnetic field (Zhang & Cui, 2022). This sets it apart from magnetic materials like iron, nickel, or cobalt, which exhibit crystal structures leading to magnetic domains and significant magnetic moments (Tian et al., 2020). The non-magnetic nature of silicon arises from its electron configuration, wherein orbitals are filled with pairs of electrons having opposite spins. With an atomic number of 14, silicon has the electron configuration $1s^2\ 2s^2\ 2p^6\ 3s^2\ 3p^2$. Consequently, all electrons at both the lowest energy level (valence band) and the subsequent energy level (conduction band) form pairs with opposite spins. This arrangement causes the magnetic moments of these electron pairs to counterbalance each other, resulting in silicon having a minimal inclination to exhibit magnetism or be influenced by an external magnetic field at the atomic level (Pamungkas et al., 2020).

Modification of silicon materials needs to be carried out to address the weaknesses related to electrical conductivity and magnetic properties, one of which involves transition metals either as alloys, composites, coatings, or doping (Feng et al., 2021; Nulu et al., 2022). Generally, transition metals have high density, melting point, boiling point, magnetic properties, and electrical conductivity (Tyagi et al., 2020). In some transition metals, there are metallic bonds with easily transferable electrons (free electrons), so the presence of transition metals in modified silicon can alter its electrical and magnetic characteristics (Li et al., 2020). One metal that can be used to enhance the characteristics of Si is cobalt (Co). This metal has a hexagonal structure with a density of 8.9 g/cm^3, a melting point of 1495°C, an electrical conductivity of 17.9×10^6 S/m, and is a ferromagnetic material (Greenwood & Earnshaw, 2012). Based on several research findings, modification using transition metals has been reported to improve the characteristics of Si, such as Ni (Ensafi et al., 2017), Fe (Chae et al., 2013), Cu (Xu et al., 2016), and Mn (Nulu et al., 2022).

This research utilizes rice husk ash as a source of SiO_2. SiO_2 is prepared using the magnesiothermic reduction method to obtain Si material. Subsequently, Co-modified Si is synthesized with varying Co concentrations (0%, 0.1%, and 0.5%) using the impregnation method. A study on the structure, morphology, electrical conductivity, and magnetic properties influenced by the Co metal concentration doped onto the Si material needs to be investigated to enhance functional characteristics and provide a solution to the incompatibility of silicon in its application.

2. METHOD

2.1 Materials and Tools

Rice husk, potassium bromide (KBr 98%, Pudak), magnesium powder (Mg, Merck), hydrochloric acid (HCl 37%, Merck), hydrofluoric acid (HF 40%, Merck), cobalt nitrate ($Co(NO_3)_2.6H_2O$, Merck), absolute ethanol, sodium hydroxide (NaOH, Merck), and deionized (DI) water (0.05 µS/cm). The equipment utilized in this research includes XRF (Rigaku), XRD (Bruker), SEM-EDX (JEOL), Magnetic Susceptibility (Bartington), Analytical balance with a precision of 0.0001 g, Furnace, Oven, pH meter, Hot plate stirrer, Whatman No. 41 filter paper, 100 mesh sieve, a set of conductometer tools, and other glassware (Pyrex).

2.2 Silicon Synthesis from Rice Husk

Rice husk was calcined at 600°C for 5 hours. Subsequently, 5 g of rice husk ash (RHA) underwent a leaching process using 100 mL 10% NaOH at 90°C for 3 hours. The obtained filtrate (sodium silicate) was titrated with 3M HCl to form a gel (pH 7) and left undisturbed for 24 hours. The silica gel was filtered, washed with DI water, and then oven-dried at 120°C for 2 hours. The extracted silica was mixed with KBr (1:10) in 150 mL of DI water. The mixture was stirred for 6 hours and followed by a decantation process. The obtained residue was heated at 80°C for 12 hours. Subsequently, the mixture was supplemented with 10 g of magnesium powder (silica-to-Mg ratio of 1:2) and annealed at 800°C under standard atmospheric conditions at a heating rate of 2°C/minute and held for 6 hours. The resulting reduced silicon underwent a purification process: the first stage involved washing the solid with 140 mL of DI water + 10 mL of ethanol, the second stage with 150 mL of 5N HCl, the third stage with 150 mL of 10% HF, and finally, the solid was washed again with DI water and dried at 80°C for 12 hours.

2.3 Co/Si Synthesis via Co-precipitation

Silicon (3 g) in a covered ceramic container was mixed with Co precursors (0.1% and 0.5%). Then, 2 mL of ethanol was added to the container. The mixture (Co/Si slurry) was stirred for 1 hour. The Co/Si composite was annealed at 400°C under standard atmospheric conditions at a rate of 2°C/minute and maintained at this temperature for 40 minutes. After heating, the furnace was left overnight at room temperature. The resulting samples were labeled Si (without cobalt), 0.1%Co/Si, and 0.5%Co/Si, and subsequently characterized using XRD, SEM-EDX-Mapping, electrical conductivity, and magnetic properties.

3. RESULTS AND DISCUSSION

3.1 Structural and Morphology Analysis

The extracted silica exhibits a solid, coarse, white form with a yield of up to 99.49% from rice husk ash (RHA). Analysis using XRF (Table 1) reveals that the extracted silica has a high Si content, reaching 99.91%. The purity of the produced silica depends on the rice husk burning process, temperature, and alkali solution concentration in the leaching process (Daulay et al., 2021). Furthermore, based on the XRD analysis in Figure 1 (a), broad peaks are observed at (2θ): 22-23°. These patterns indicate that the silica possesses an amorphous phase. The same XRD pattern is also confirmed by (Kaleli et al., 2020).

Table 1 Chemical composition of rice husk ash and silica by XRF method.

Element	RHA (%Wt)	Silica (% Wt)
Si	97,09	99,91
Fe	0,14	0,04
Ni	0,03	0,02
Cu	0,01	0,01
Zn	0,02	0,01

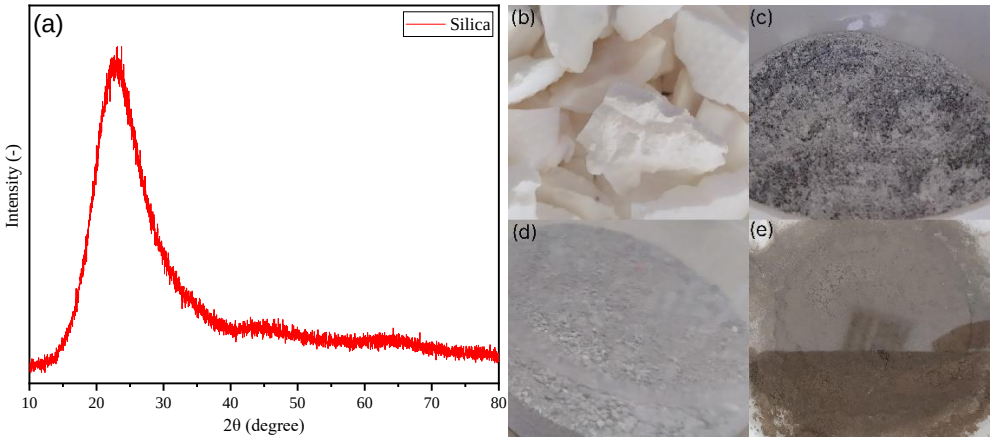

Figure 1. (a) Silica diffractogram, (b) extracted silica, (c) silica and Mg mixture before reduction, (d) silicon after reduction, and (e) purified silicon

The silica is further transformed into silicon using the magnesiothermic reduction method. In this process, KBr salt is utilized as a heat sink during the magnesiothermic reduction process, aiming to prevent agglomeration and facilitate the formation of a 3D silicon network (Andriayani et al., 2014; Daulay et al., 2022). The heat of fusion of KBr (ΔH_{fusion}) is known to be 25.5 kJ/mol, while the heat generated from the magnesiothermic reduction (Mg(g)) ΔH = -586.7 kJ/molSiO_2. Therefore, the excess heat is utilized for the fusion of KBr, preventing silicon agglomeration (Dworkin & Bredig, 1960; Favors et al., 2014; Redkin et al., 2018). During the reduction process leading to silicon formation, simultaneous by-products such as MgO and Mg_2Si are produced. Hence, purification of the synthesized silicon product is necessary through washing with DI H_2O + EtOH, HCl, and HF. Silicon is repeatedly washed with DI H_2O + EtOH to remove KBr salt. HCl is employed to eliminate Mg, Mg_2Si, and MgO, while HF is used to remove some unreduced SiO_2. The silicon obtained after purification of the reduction exhibited a brownish powder color, as depicted in figure 1 (e). Similar observations were reported by Favors et al. (2014), who utilized NaCl salt in the magnesiothermic reduction process. Subsequently, the reduce silicon was doped with cobalt (Co) metal to enhance the characteristics of the silicon material. Notably, there is no significant change was observed in the resulting solid powder, which maintained its brownish color.

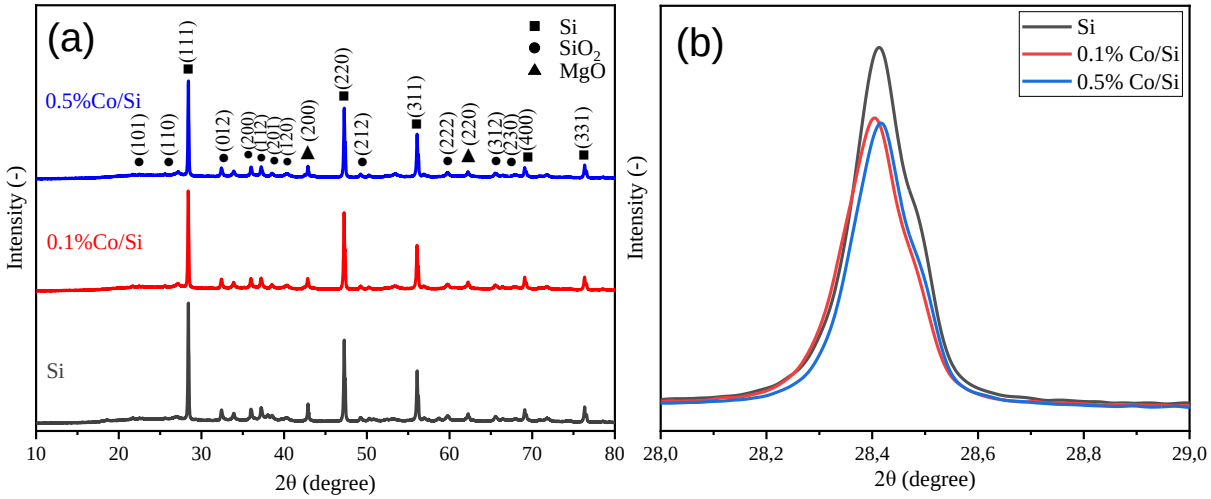

Figure 2. (a) Diffractogram Si and Co/Si, (b) magnified of Si peak (111) at 28,4°.

The XRD analysis indicates a phase change in Si from the raw silica material, which initially had an amorphous phase, to a crystalline phase. The XRD diffractogram of Si and Co/Si samples presented in Figure 2 shows characteristic silicon diffraction patterns (JCPDS Card No. 00-026-1481)

at 2θ angles of 28.42º, 47.28º, 56.11º, 69.13º, and 76.36º, corresponding to the reference hkl values (111), (220), (311), (400), and (331) (Daulay et al., 2022; Zuo et al., 2022). The produced material exhibits a high level of crystallinity after the heating and purification treatments, with low concentrations of by-products such as SiO_2 (Cristobalite) and MgO (Periclase) still present. Furthermore, Rietveld analysis for the 0.1%Co/Si and 0.5%Co/Si materials did not exhibit peaks related to Co doping, which could be due to their low doping concentrations. Additionally, no new impurity peaks such as Co oxides and Co silicides were detected, indicating the successful doping of Co into Si (Nulu et al., 2021). The enlargement of the peak at 28.4° (111) in Figure 2 (a), as shown in Figure 2 (b), demonstrates that the peak intensity decreased as the concentration of Co dopant increased, indicating a reduction in the crystallinity of Si due to the incorporation of Co atoms. The peak intensity for 0.5%Co/Si is lower than that for 0.1%Co/Si, indicating a significant amount of Co doping within the Si lattice. This decrease in intensity can be associated with the larger ionic radius of Co compared to Si, ultimately causing expansion in the lattice distance or lattice distortion in the crystal structure of Si due to the presence of doped Co atoms (Kobayashi et al., 2018; Nulu et al., 2022). The lattice distortion implies that the arrangement of Si atoms is not in the ideal position, or there is a deviation from the regular arrangement within the crystal lattice (Kumar et al., 2023). Besides the influence of the Co dopant, high temperature is also one of the factors affecting lattice distortion (Ding et al., 2023). Lattice distortion in the crystal structure can affect crystal properties such as electrical conductivity, thermal conductivity, mechanical properties, magnetic properties, and can also influence the optical properties of the crystal (Ding et al., 2023; Kumar et al., 2023).

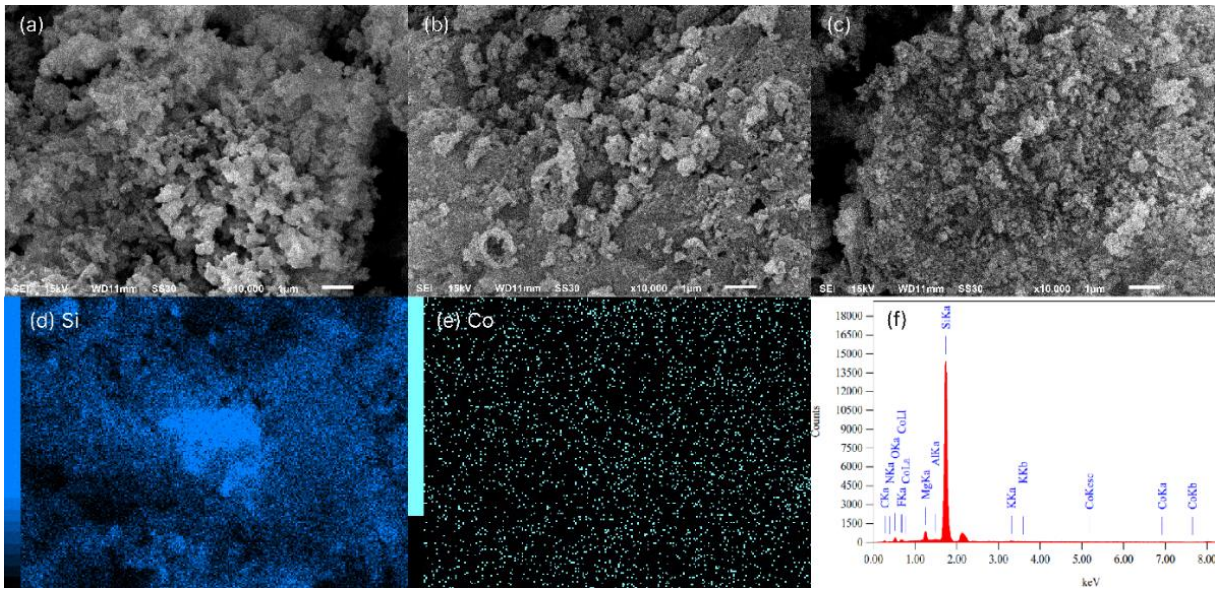

Figure 3. SEM morphology (a) Si, (b) 0.1%Co/Si, (c) 0.5%Co/Si, elemental mapping (d) Si and (e) Co on 0.5%Co/Si, (f) EDX results on 0.5%Co/Si.

Table 3. Abundance of elements in Si and Co/Si from EDX analysis

Element	Si			0.1%Co/Si			0.5%Co/Si		
	Mass%	Atom%	Sigma	Mass%	Atom%	Sigma	Mass%	Atom%	Sigma
Si	31,44	20,22	0,15	25,07	15,69	0,16	26,35	17,01	0,15
Co	-	-	-	0,27	0,08	0,06	0,69	0,21	0,08
O	19,43	21,94	0,22	40,83	44,87	0,34	23,43	26,55	0,25
Mg	12,35	9,18	0,09	3,93	2,84	0,07	15,45	11,52	0,11
N	21,85	28,17	0,31	16,62	20,87	0,29	20,28	26,26	0,31
C	11,79	17,73	0,14	7,60	11,12	0,12	10,06	15,18	0,13
K	0,44	0,20	0,03	0,98	0,44	0,04	0,55	0,26	0,04

Subsequently, an analysis of the morphology of Si and Co/Si was conducted using SEM. Figure 3 (a, b, c) shows the morphology of Si and Co/Si at a scale of 1 µm, displaying rough, uneven, and porous surfaces with particles appearing spherical and varying in size. The morphological appearance does not exhibit significant differences with the addition of Co metal. This may be attributed to the very low concentration of Co metal doping, resulting in the morphology being predominantly influenced by the silicon surface. The morphology in each sample reveals interconnected patterns. This is because the magnesiothermic reduction temperature plays a crucial role in controlling the silicon structure (Zuo et al., 2022). Subsequently, EDX analysis and elemental mapping were performed to confirm the presence of Co metal in each Co/Si variation. Table 3 shows the existence of Co metal in 0.1%Co/Si at 0.27% and 0.5%Co/Si at 0.69%. The obtained values are higher than their theoretical values, indicating that some Co metal is localized on the silicon surface. This phenomenon may be caused by differences in surface tension, leading to Co metal aggregation in specific areas on the silicon surface (Qiu et al., 2020). Meanwhile, Sihombing et al. (2020) reported differences between theoretical values and EDX analysis results, which could be due to low-resistance phase. Elemental mapping results for 0.5%Co/Si (Figure 3.d-e) indicate the presence of Co metal scattered on the synthesized Si material surface. This confirms that Co metal has successfully been doped into the Si crystal.

3.2 Electrical Conductivity Analysis

Electrical conductivity testing was conducted to determine the ability of Si and Co/Si to conduct electric current. Electrical conductivity measurements were conducted by placing Si and Co/Si materials into a conductivity cell and subsequently measuring the electrical conductivity using a conductivity meter. The data from the electrical conductivity measurements are presented in Figure 4. The electrical conductivity value obtained for Si was 1223.24 µS/cm. Furthermore, the analysis results indicate that the addition of Co metal positively influences the electrical conductivity through charge-carrier doping, introducing extra electrons to the silicon crystal lattice. This mechanism increases the concentration of free electrons within the material, thereby enhancing its electrical conductivity. The interaction between Co and Si facilitates the creation of donor level within the band structure, contributing to the modification of electronic properties (Rhaman et al., 2020; Bystrický et al., 2023). The increase in electrical conductivity is proportional to the concentration of Co metal doping, with conductivity values obtained for the 0.1%Co/Si variation at 1376.15 µS/cm and for 0.5%Co/Si at 1529.05 µS/cm. The observed enhancement aligns with that of C. Xu et al. (2016), indicated that the Cu metal on the $Si_{85}Cu_{15}$ composite can significantly increase the electrical conductivity by up to 75.24% and reduce the resistance of Si from 269.2 Ω to 153.6 Ω. This result also clarifies that the addition of Co metal can modify the electronic properties of Si material and produce n-type (negative) semiconductors where electrical conduction is dominated by electrons (Salem et al., 2023).

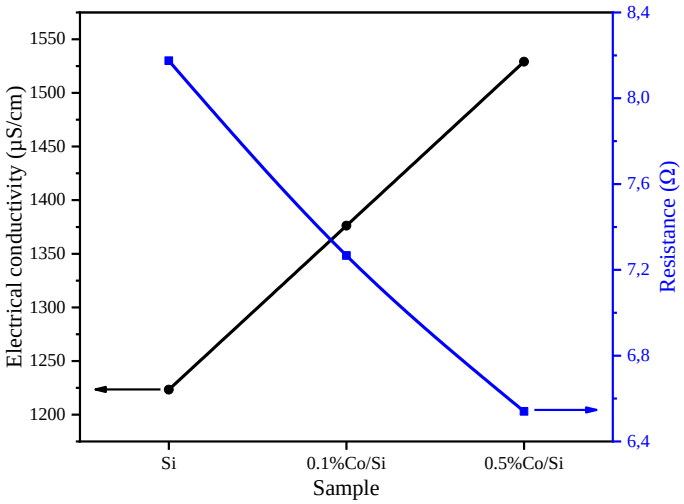

Figure 4. Graph of electrical conductivity and resistance of Si and Co/Si.

3.3 Magnetic Susceptibility Analysis

Furthermore, based on the results of magnetic susceptibility analysis shown in Figure 5, it is known that silica and RHA samples have negative values. This indicates that silica and RHA are materials that repel an external magnetic field or exhibit diamagnetic properties (Nakashima, 2020). However, Si shows a positive magnetic susceptibility value of 1.81E-6. This indicates the interaction between silicon oxide and magnesium in the magnesiothermic reduction process, which not only changes the crystal structure of silicon but also alters the magnetic properties, leading to an increase in paramagnetism (Ding et al., 2023; Kumar et al., 2023). Additionally, the presence of magnesium also influences the magnetic properties due to its paramagnetic nature (Gaeta et al., 2021). Furthermore, the addition of Co metal dopant into Si material can also increase the magnetic susceptibility value. The higher the concentration of Co, the greater its contribution to the overall material susceptibility. This phenomenon can occur because of the inherent ferromagnetic nature of Co, which naturally organizes the magnetic domains in a specific direction under the influence of an external magnetic field (Greenwood & Earnshaw, 2012; Guo et al., 2021). The addition of Co dopant affects the crystal growth and material structure, causing the distributed atoms in the material matrix to interact with each other. This interaction leads to the arrangement of more organized magnetic domains, resulting in a larger magnetic susceptibility (Dhanalakshmi et al., 2023). The improvement in electrical conductivity and magnetic properties of this modified silicon material has significant implications for the development of semiconductor components, sensors, diodes, batteries, transistors, and photovoltaic devices.

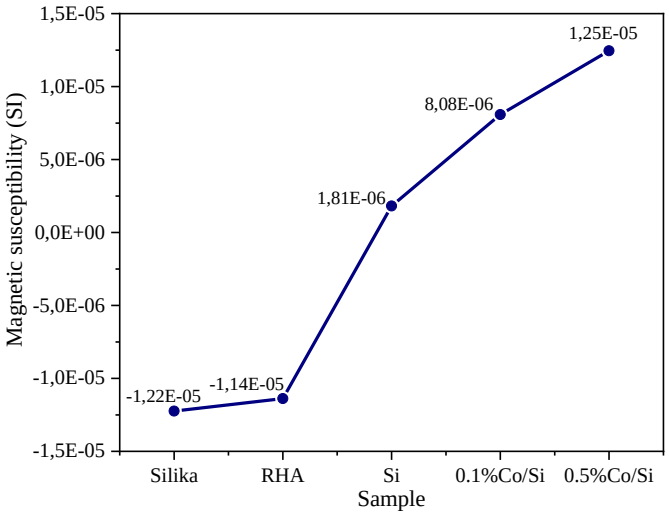

Figure 5. Magnetic susceptibility of Si and Co/Si.

4. CONCLUSION

The modification of silicon resulting from magnesiothermic reduction using Co metal dopant through the impregnation method has been successfully conducted significantly enhancing the electrical conductivity and magnetic properties of the silicon material. The modification of the Si material resulted an increasing trend in electrical conductivity values by 12.51% in 0.1%Co/Si and 25.02% in 0.5%Co/Si. Furthermore, there was an increase in magnetic susceptibility values to 8.08 x 10^{-6} SI in 0.1%Co/Si and 1.25 x 10^{-5} SI in 0.5%Co/Si. These results indicate that Si material doped with Co metal provides insights into an effective and cost-effective approach applicable to production of high-performance Si-based materials for the development of semiconductor, batteries, sensors, and optical technology.

ACKNOWLEDGEMENT

The authors acknowledge to the Laboratory Faculty of Science and Technology for support and contribution this research of the Master's degree program.

REFERENCE

Andriayani, Sofyan, N., Sihotang, H., & Raja, S. L. (2014). Increased of Purity Silicon from Natural Sand with Variation of Heating Time through Magnesiotermal. *Proceedings of the 2nd International Conference on Natural and Environmental Sciences (ICONES)*, 149–154.

Baig, N., Kammakakam, I., Falath, W., & Kammakakam, I. (2021). Nanomaterials: A review of synthesis methods, properties, recent progress, and challenges. *Materials Advances*, *2*(6), 1821–1871. https://doi.org/10.1039/d0ma00807a

Bystrický, R., Škrátek, M., Rusnák, J., Precner, M., Ťapajna, M., Hnatko, M., & Šajgalík, P. (2023). Electrical and magnetic properties of silicon carbide composites with titanium and niobium carbide as sintering aids. *Ceramics International*, *49*(3), 5319–5326. https://doi.org/https://doi.org/10.1016/j.ceramint.2022.10.055

Chae, S., Ko, M., Park, S., Kim, N., Ma, J., & Jaephil, C. (2013). Micron-Sized Fe-Cu-Si Ternary Composite Anodes for High Energy Li-ion Batteries. *Energy & Environmental Science*. https://doi.org/10.1039/b000000x

Daulay, A., Andriayani, Marpongahtun, & Gea, S. (2021). Extraction silica from rice husk with naoh leaching agent with temperature variation burning rice husk. *Rasayan Journal of Chemistry*, *14*(3), 2125–2128. https://doi.org/10.31788/RJC.2021.1436351

Daulay, A., Andriayani, Marpongahtun, & Gea, S. (2022). Synthesis and application of silicon nanoparticles prepared from rice husk for lithium-ion batteries. *Case Studies in Chemical and Environmental Engineering*, *6*(July), 100256. https://doi.org/10.1016/j.cscee.2022.100256

Dhanalakshmi, B., Sravani, G. M., Suresh, J., Reddy, P. V. S. S. S. N., Rao, K. E., Jyothula, S., & Beera, C. S. (2023). Impact of co-doping with Mn and Co/Mn on the structural, microstructural, dielectric, impedance, and magnetic characteristics of multiferroic bismuth ferrite nanoparticles. *Applied Physics A*, *129*(6), 452. https://doi.org/10.1007/s00339-023-06737-4

Ding, N., Jiang, H.-H., Xu, C.-R., Shao, L., & Tang, B.-Y. (2023). Lattice distortion, mechanical and thermodynamic properties of (TiZrHf)C and (TiZrHf)N ceramics. *Applied Physics A*, *129*(10), 720. https://doi.org/10.1007/s00339-023-06983-6

Dohnalová, K., & Kůsová, K. (2021). *Optical Properties of Si Nanocrystals Enhanced by Ligands BT - Silicon Photonics IV: Innovative Frontiers* (D. J. Lockwood & L. Pavesi (eds.); pp. 3–65). Springer International Publishing. https://doi.org/10.1007/978-3-030-68222-4_1

Dworkin, A. S., & Bredig, M. A. (1960). The heats of fusion of the alkali metal halides. *The Journal of Physical Chemistry*, *64*(2), 269–272. https://doi.org/10.1021/j100831a023

Ensafi, A. A., Abarghoui, M. M., & Rezaei, B. (2017). Metal (Ni and Bi) coated porous silicon nanostructure, high-performance anode materials for lithium ion batteries with high capacity and stability. *Journal of Alloys and Compounds*, *712*, 233–240. https://doi.org/10.1016/j.jallcom.2017.04.103

Favors, Z., Wang, W., Bay, H. H., Mutlu, Z., Ahmed, K., Liu, C., Ozkan, M., & Ozkan, C. S. (2014). Scalable synthesis of nano-silicon from beach sand for long cycle life Li-ion batteries. *Scientific Reports*, *4*, 1–7. https://doi.org/10.1038/srep05623

Feng, Z., Peng, W., Wang, Z., Guo, H., Li, X., Yan, G., & Wang, J. (2021). Review of silicon-based alloys for lithium-ion battery anodes. *International Journal of Minerals, Metallurgy and Materials*, *28*(10), 1549–1564. https://doi.org/10.1007/s12613-021-2335-x

Gaeta, M., Cavallaro, M., Vinci, S. L., Mormina, E., Blandino, A., Marino, M. A., Granata, F., Tessitore, A., Galletta, K., D'Angelo, T., & Visalli, C. (2021). Magnetism of materials: theory and practice in magnetic resonance imaging. *Insights into Imaging*, *12*(1), 179. https://doi.org/10.1186/s13244-021-01125-z

Greenwood, N. N., & Earnshaw, A. (2012). *Chemistry of the Elements*. Elsevier.

Guo, Y., Zhou, S., & Zhao, J. (2021). Two-dimensional intrinsic ferromagnets with high Curie temperatures: synthesis, physical properties and device applications. *Journal of Materials Chemistry C*, *9*(19), 6103–6121. https://doi.org/10.1039/D1TC00415H

Kaleli, M. J., Kamweru, P. K., Gichumbi, J. M., & Ndiritu, F. G. (2020). Characterization of rice husk ash prepared by open air burning and furnace calcination. *Journal of Chemical Engineering and Materials Science*, *11*(2), 24–30. https://doi.org/10.5897/jcems2020.0348

Kiran, S. K., Ramesh, M., Shukla, S., & Saxena, S. (2020). Silicon Materials for Lithium-ion Battery Applications. In *Materials Research Foundations* (Issue 80, pp. 161–202). https://doi.org/10.21741/9781644900918-1

Kobayashi, S., Ikuhara, Y., & Mizoguchi, T. (2018). Lattice expansion and local lattice distortion in Nb- and La-doped SrTiO3 single crystals investigated by x-ray diffraction and first-principles calculations. *Physical Review B*, *98*(13), 134114. https://doi.org/10.1103/PhysRevB.98.134114

Kumar, D., & Johari, M. (2020). Characteristics of silicon crystal, its covalent bonding and their structure, electrical properties, uses. In *AIP Conference Proceedings* (Vol. 2220). https://doi.org/10.1063/5.0003505

Kumar, J., Linda, A., & Biswas, K. (2023). Lattice distortion in FCC HEAs and its effect on mechanical properties: Critical analysis and way forward. *Journal of Applied Physics*, *133*(15), 155102. https://doi.org/10.1063/5.0144456

Li, S., Wang, J., Ye, Y., Tang, Y., Li, X., Gu, F., & Li, L. (2020). Composite Si-O-metal network catalysts with uneven electron distribution: Enhanced activity and electron transfer for catalytic ozonation of carbamazepine. *Applied Catalysis B: Environmental*, *263*, 118311. https://doi.org/https://doi.org/10.1016/j.apcatb.2019.118311

Margalit, N., Xiang, C., Bowers, S. M., Bjorlin, A., Blum, R., & Bowers, J. E. (2021). Perspective on the future of silicon photonics and electronics. *Applied Physics Letters*, *118*(22). https://doi.org/10.1063/5.0050117

Nakashima, R. (2020). Diamagnetic levitation of a milligram-scale silica using permanent magnets for the use in a macroscopic quantum measurement. *Physics Letters A*, *384*(24), 126592. https://doi.org/https://doi.org/10.1016/j.physleta.2020.126592

Ng, K. K. (2002). *Complete Guide to Semiconductor Devices, Second Edition*. John Wiley & Sons. https://doi.org/10.1002/9781118014769

Nulu, A., Nulu, V., & Sohn, K. Y. (2021). Effect of Cobalt Doping on Enhanced Lithium Storage Performance of Nanosilicon. *ChemElectroChem*, *8*(7), 1259–1269. https://doi.org/10.1002/celc.202001533

Nulu, A., Nulu, V., & Sohn, K. Y. (2022). Influence of transition metal doping on nano silicon anodes for Li-ion energy storage applications. *Journal of Alloys and Compounds*, *911*, 164976. https://doi.org/10.1016/j.jallcom.2022.164976

Pamungkas, M. A., Sari, F., Abdurrouf, & Nurhuda, M. (2020). Magnetic properties of Ga-doped and As-doped hydrogenated silicene: Density Functional Theory (DFT) calculations. *Journal of Physics: Conference Series*, *1572*(1). https://doi.org/10.1088/1742-6596/1572/1/012043

Qiu, C., Odarchenko, Y., Meng, Q., Cong, P., Schoen, M. A. W., Kleibert, A., Forrest, T., & Beale, A. M. (2020). Direct observation of the evolving metal-support interaction of individual cobalt nanoparticles at the titania and silica interface. *Chemical Science*, *11*(48), 13060–13070. https://doi.org/10.1039/d0sc03113e

Redkin, A., Korzun, I., Reznitskikh, O., Yaroslavtseva, T., Zaikov, Y., & Kumkov, S. (2018). Heat of fusion of halide salts and their eutectics. *Journal of Thermal Analysis and Calorimetry*, *131*(2), 2021–2026. https://doi.org/10.1007/s10973-017-6650-4

Rhaman, M. M., Matin, M. A., Al Mamun, M. A., Hussain, A., Hossain, M. N., Das, B. C., Hakim, M. A., & Islam, M. F. (2020). Enhanced electrical conductivity and multiferroic property of cobalt-doped bismuth ferrite nanoparticles. *Journal of Materials Science: Materials in Electronics*, *31*(11), 8727–8736. https://doi.org/10.1007/s10854-020-03407-6

Saif, O. M., Zekry, A. H., Abouelatta, M., & Shaker, A. (2023). A Comprehensive Review of Tandem Solar Cells Integrated on Silicon Substrate: III/V vs Perovskite. *Silicon*, *15*(15), 6329–6347. https://doi.org/10.1007/s12633-023-02466-8

Salem, M. A., Talla, J. A., & Al-Moumani, A. L. (2023). Electronic and Magnetic Properties of Doped Silicon Carbide Nanosheet Under an External Electric Field. *International Journal of Theoretical Physics*, *62*(7), 137. https://doi.org/10.1007/s10773-023-05415-8

Sihombing, J. L., Gea, S., Wirjosentono, B., Agusnar, H., Pulungan, A. N., Herlinawati, H., & Yusuf, M. (2020). Characteristic and Catalytic Performance of Co and Co-Mo Metal Impregnated in Sarulla Natural Zeolite Catalyst for Hydrocracking of MEFA Rubber Seed Oil into Biogasoline Fraction. *Catalysts*, *10*, 121.

Tan, C. S. (2022). Density Functional Theory Study of Metallic Silicon (111) Plane Structures. *ACS Omega*, *7*(6), 5385–5392. https://doi.org/10.1021/acsomega.1c06614

Tan, Y., Jiang, T., & Chen, G. Z. (2021). Mechanisms and Product Options of Magnesiothermic Reduction of Silica to Silicon for Lithium-Ion Battery Applications. *Frontiers in Energy Research*, *9*(March), 1–19. https://doi.org/10.3389/fenrg.2021.651386

Thio, P. R., Koffi, K. B., Konan, K. D., & Yao, K. A. (2021). Production of High-Purity Silica Sand from Ivorian Sedimentary Basin by Attrition without Acid Leaching Process for Windows Glass Making. *Journal of Minerals and Materials Characterization and Engineering*, *09*(04), 345–361. https://doi.org/10.4236/jmmce.2021.94024

Tian, Y., Zhu, Z., Ge, Z., Sun, A., Zhang, Q., Huang, S., Li, H., & Meng, J. (2020). Electronic and magnetic properties of 3d transition metal doped MoSe2 monolayer. *Physica E: Low-Dimensional Systems and Nanostructures*, *116*, 113745. https://doi.org/https://doi.org/10.1016/j.physe.2019.113745

Tyagi, A., Banerjee, S., Cherusseri, J., & Kar, K. K. (2020). *Characteristics of Transition Metal Oxides BT - Handbook of Nanocomposite Supercapacitor Materials I: Characteristics* (K. K. Kar (ed.); pp. 91–123). Springer International Publishing. https://doi.org/10.1007/978-3-030-43009-2_3

Xu, C., Hao, Q., & Zhao, D. (2016). Facile fabrication of a nanoporous Si/Cu composite and its application as a high-performance anode in lithium-ion batteries. *Nano Research*, *9*(4), 908–916.

https://doi.org/10.1007/s12274-015-0973-x

Xu, Z. L., Liu, X., Luo, Y., Zhou, L., & Kim, J. K. (2017). Nanosilicon anodes for high performance rechargeable batteries. *Progress in Materials Science*, *90*(July), 1–44. https://doi.org/10.1016/j.pmatsci.2017.07.003

Zhang, L., & Cui, Z. (2022). *Electronic , Magnetic , and Optical Performances of Non-Metals Doped Silicon Carbide*. *10*(April), 1–8. https://doi.org/10.3389/fchem.2022.898174

Zuo, X., Yang, Q., He, Y., Cheng, Y. J., Yin, S., Zhu, J., Müller-Buschbaum, P., & Xia, Y. (2022). High-Temperature Magnesiothermic Reduction Enables HF-Free Synthesis of Porous Silicon with Enhanced Performance as Lithium-Ion Battery Anode. *Molecules*, *27*(21). https://doi.org/10.3390/molecules27217486